

# Synthesis and Microwave Dielectric Properties of $A_{16}V_{18}O_{61}$ (A = Ba, Sr and Ca) Ceramics for LTCC Applications

E.K. SURESH,<sup>1</sup> K. PRASAD,<sup>1</sup> N.S. ARUN,<sup>1</sup> and R. RATHEESH<sup>1,2</sup>

1.—Department of Information Technology, Government of India, Microwave Materials Group, Centre for Materials for Electronics Technology (C-MET), Thrissur, Kerala 680581, India.  
2.—e-mail: ratheeshr@yahoo.com

Low-temperature co-firable  $A_{16}V_{18}O_{61}$  (A = Ba, Sr, Ca) ceramics have been prepared through the solid state ceramic route. The structural features of these ceramics have been studied using the x-ray diffraction (XRD) technique. The existence of the  $A_{16}V_{18}O_{61}$  (A = Ba, Sr, Ca) ceramic phase was confirmed through laser Raman spectroscopic studies. Scanning electron microscopy analysis revealed a dense microstructure for the ceramics with closely packed polygonal grains. Among the samples studied,  $Ba_{16}V_{18}O_{61}$  ceramic was prepared in the ultralow sintering temperature of 620°C for 1 h, which can be co-firable with an aluminium electrode. XRD and electron dispersive spectroscopy analyses showed that the samples under study have excellent compatibility with metal electrodes. The microwave dielectric properties measured using a vector network analyzer revealed that  $A_{16}V_{18}O_{61}$  (A = Ba, Sr, Ca) ceramics have excellent unloaded quality factors.

**Key words:** Ceramics, sintering, Raman spectroscopy, dielectric properties

## INTRODUCTION

Low-temperature cofired ceramic (LTCC) technology has exhibited incredible growth in the past few decades, due to its tremendous application potential in the wireless communication industry. Miniaturization of circuit dimensions and integration of more components in a small volume are the great challenges encountered in the modern circuit fabrication industry. LTCC technology is one of the most promising packaging technologies, since it provides high-density circuit packaging, high reliability and low circuit resistance. The wireless communication industry demands microwave dielectric ceramics with low dielectric constant for high-speed signal propagation, high-quality factors for better selectivity and a near-zero temperature coefficient of resonant frequency for stability of operation. In addition to this, low sintering temperature and chemical compatibility with metal electrodes such as Ag, Al, etc. are also mandatory features required for LTCC materials. Glass addition and proper selection of low melting oxide compositions

are the two approaches generally employed for reducing the sintering temperature of conventional microwave ceramic materials.<sup>1–3</sup> However, these approaches are not preferred due to their adverse effect on the quality factor of microwave ceramics.

Development of single phase materials which can be sintered at very low temperatures (<650°C) is the latest trend in LTCC technology. The continuous efforts in this direction have resulted in a new class of materials known as ultra-low-temperature co-fired ceramics (ULTCC), wherein the base ceramic composition sinters at temperatures lower than the melting point of the electrode material, i.e. aluminium (660°C).<sup>4,5</sup> Recent studies have shown that  $TeO_2$ -,  $Bi_2O_3$ -,  $MoO_3$ - and  $V_2O_5$ -based material systems are suitable for the development of ULTCC ceramics, because of their low sintering temperature.<sup>6–9</sup> Although tellurites can be sintered at very low temperatures, their high cost, toxic nature, and reactivity with metal electrodes limit their wider use in ULTCC technology.<sup>10</sup> Molybdate- and vanadate-based compositions exhibited low sintering temperatures and low dielectric constant compared to  $Bi_2O_3$ -based systems.<sup>11</sup>

In view of the above, single phase  $MoO_3$ - and  $V_2O_5$ -based material systems have been prepared by many researchers and studied for their suitability for microwave applications.<sup>12–15</sup> Recently, we have reported  $Ba_3V_4O_{13}$  and  $BaV_2O_6$  ceramics with ultra-low sintering temperatures together with superior microwave dielectric properties and good chemical compatibility with Al electrodes.<sup>4,16</sup> In the present study, the structure and microwave dielectric properties of a vanadium-based  $A_{16}V_{18}O_{61}$  (A = Ba, Sr, Ca) ceramics system has been investigated with a view to use it for LTCC and ULTCC applications.

## EXPERIMENTAL PROCEDURE

The  $A_{16}V_{18}O_{61}$  (A = Ba, Sr, Ca) ceramics were prepared through the solid state ceramic route. High-purity  $BaCO_3$  (99%; Sigma Aldrich),  $SrCO_3$  (99%; Himedia),  $CaCO_3$  (99%; Sigma Aldrich) and  $V_2O_5$  (99.6%; Sigma Aldrich) were used as the starting materials. The stoichiometric amounts of oxides and carbonates were weighed and wet mixed in distilled water for about an hour and then dried in a hot-air oven at 80°C. The  $A_{16}V_{18}O_{61}$  ceramics were calcined at 550°C for 3 h in a programmable SiC furnace. The calcined compositions were ground into fine powders and 5 wt.% polyvinyl alcohol (PVA) solution was added to these powders and then dried. The powders were again well ground and pressed uniaxially in a tungsten carbide die of 11 mm diameter by applying a pressure of 250 MPa. The cylindrical compacts of the  $A_{16}V_{18}O_{61}$  samples were sintered at different temperatures for 1 h. The density of the sintered pellets was determined using the dimensional method. The phase purity of the specimens was analyzed using the x-ray diffraction technique (Bruker, Germany). The Raman spectra of the  $A_{16}V_{18}O_{61}$  ceramics were recorded using a Thermo Scientific DXR with a Nd:YVO<sub>4</sub> diode-pumped solid-state (DPSS) laser of 532 nm. The sintered ceramic compacts were thermally etched at a temperature 100°C less than that of the sintering temperature for SEM characterization. The secondary electron images and energy dispersive spectroscopy (EDS) analysis of the samples were studied using a scanning electron microscope interfaced with EDS system (SU6600; Hitachi, Japan). The linear thermal expansion coefficient of the ceramics were studied in the temperature range 30–400°C using a EXSTAR 6000 model thermomechanical analyzer (SII Nanotechnology, Japan). The dielectric constant and the unloaded quality factor of the sintered samples were studied by the Hakki and Coleman<sup>17</sup> post-resonator technique and the resonant cavity method,<sup>18</sup> respectively, using a vector network analyzer (E8362b; Agilent, USA). The temperature coefficient of resonant frequency ( $\tau_f$ ) was measured in the temperature range 30–100°C.

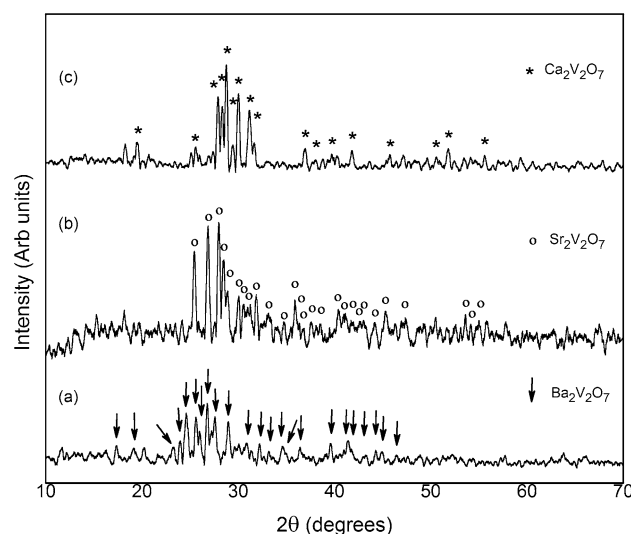


Fig. 1. X-ray diffraction patterns of (a) BVO, (b) SVO and (c) CVO ceramics sintered at 620°C, 660°C and 680°C for 1 h.

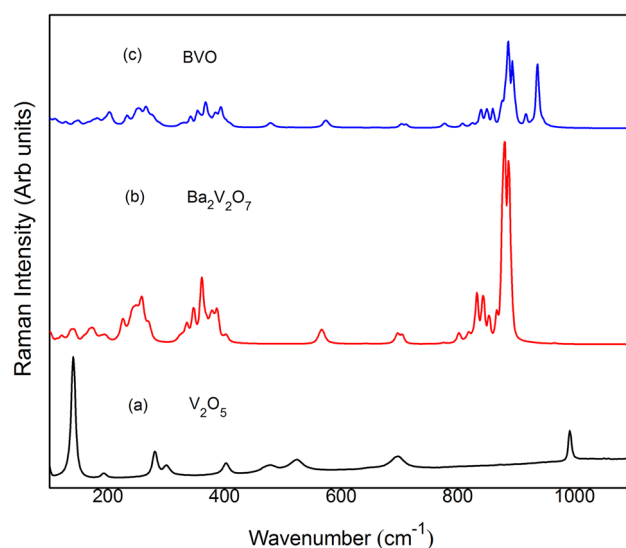


Fig. 2. Raman spectra of (a)  $V_2O_5$  powder, (b)  $Ba_2V_2O_7$  and (c) BVO ceramics.

## RESULTS AND DISCUSSION

The powder x-ray diffraction patterns of  $Ba_{16}V_{18}O_{61}$  (BVO),  $Sr_{16}V_{18}O_{61}$  (SVO) and  $Ca_{16}V_{18}O_{61}$  (CVO) ceramics sintered at 620°C, 660°C, and 680°C for 1 h, respectively, are shown in Fig. 1. Among these, the crystal structure of  $Sr_{16}V_{18}O_{61}$  (JCPDS file no: 23-0555) is reported as monoclinic with diffraction peaks close to that of  $Sr_2V_2O_7$ . The 2 theta values of the SVO ceramic in the present study does not match with the available JCPDS file (23-0555); however, it shows similarities with  $Sr_2V_2O_7$  (JCPDS file no: 32-1268). Similar results were also obtained for the BVO and CVO

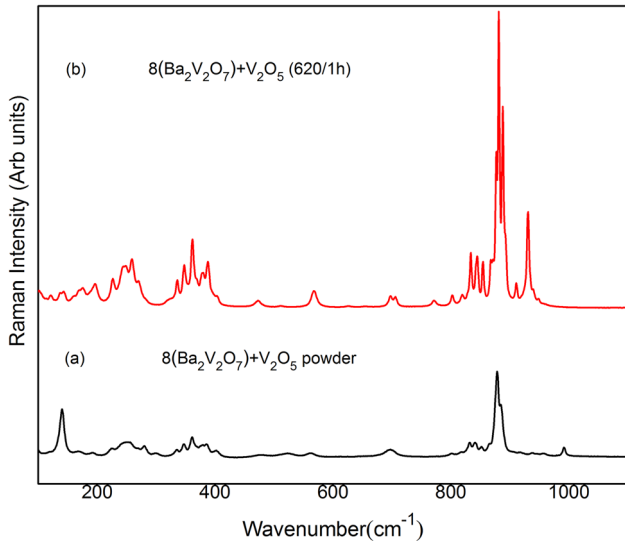


Fig. 3. Raman spectra of (a)  $8(\text{Ba}_2\text{V}_2\text{O}_7) + \text{V}_2\text{O}_5$  powder, (b)  $8(\text{Ba}_2\text{V}_2\text{O}_7) + \text{V}_2\text{O}_5$  pellet sintered at 620°C for 1 h.

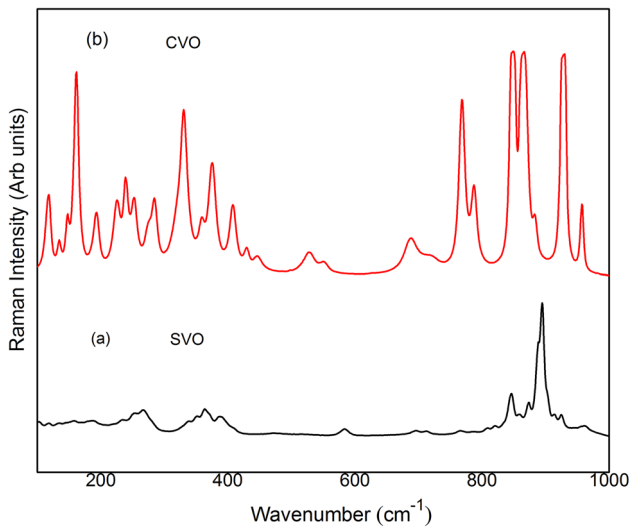


Fig. 4. Raman spectra of (a) SVO and (b) CVO ceramics sintered at 660°C and 680°C for 1 h.

ceramics and the XRD patterns of these samples also show close resemblance with the  $\text{Ba}_2\text{V}_2\text{O}_7$  and  $\text{Ca}_2\text{V}_2\text{O}_7$  ceramics.

In order to study the structure of these materials in detail, laser Raman spectroscopic studies were carried out for all the samples. Figure 2a–c shows the Raman spectra of BVO,  $\text{Ba}_2\text{V}_2\text{O}_7$  and the as-received  $\text{V}_2\text{O}_5$ . The Raman spectrum of the BVO ceramic obtained in the present study shows similar vibrational features as that of  $\text{Ba}_2\text{V}_2\text{O}_7$ .<sup>19,20</sup> The strong Raman bands observed in the BVO ceramic at 886 cm<sup>-1</sup> and 893 cm<sup>-1</sup> matches with the  $\text{Ba}_2\text{V}_2\text{O}_7$  ceramic. The Raman spectrum of the BVO ceramic consists of two additional symmetric

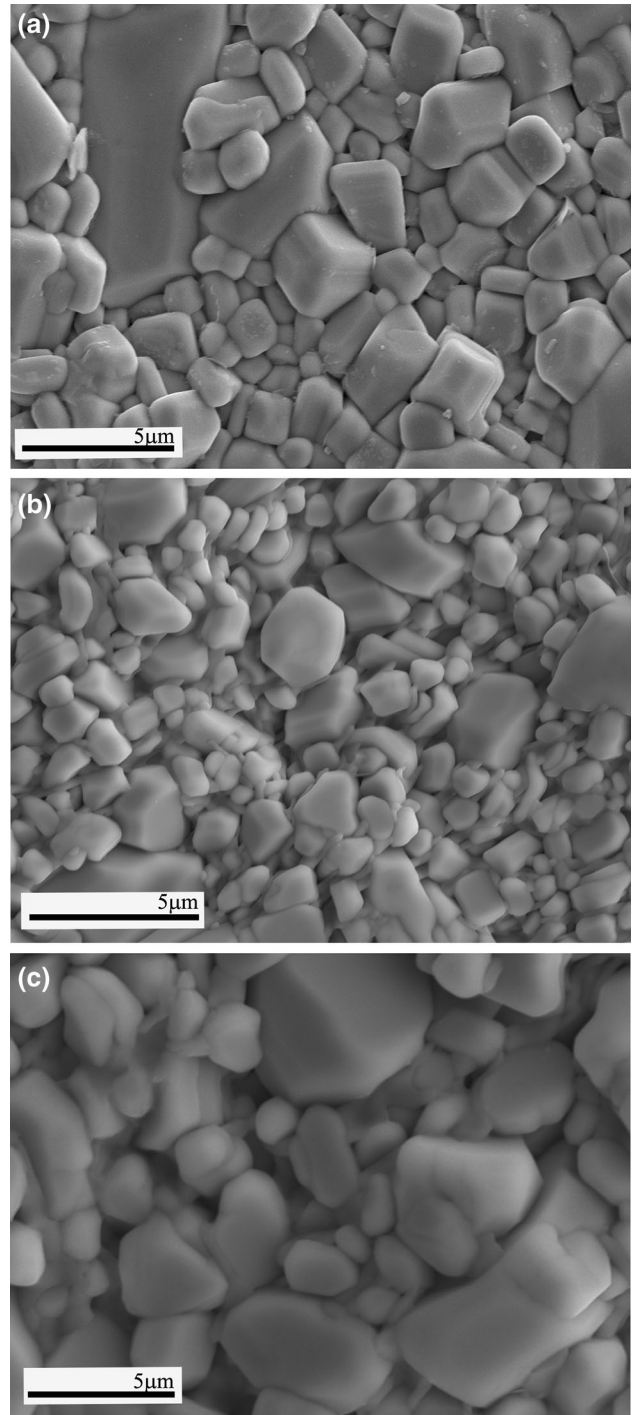


Fig. 5. SEM images of (a) BVO, (b) SVO and (c) CVO ceramics sintered at 620°C, 660°C and 680°C, respectively, for 1 h.

stretching vibrations at 916 cm<sup>-1</sup> and 936 cm<sup>-1</sup>, which are not seen in  $\text{Ba}_2\text{V}_2\text{O}_7$ . The stretching vibration of the V–O–V band at 567 cm<sup>-1</sup> and bending vibrations at 700 cm<sup>-1</sup> and 706 cm<sup>-1</sup> in the  $\text{Ba}_2\text{V}_2\text{O}_7$  ceramic are also observed in the BVO ceramic, whereas an additional symmetric bending vibration mode is observed at 478 cm<sup>-1</sup>. The

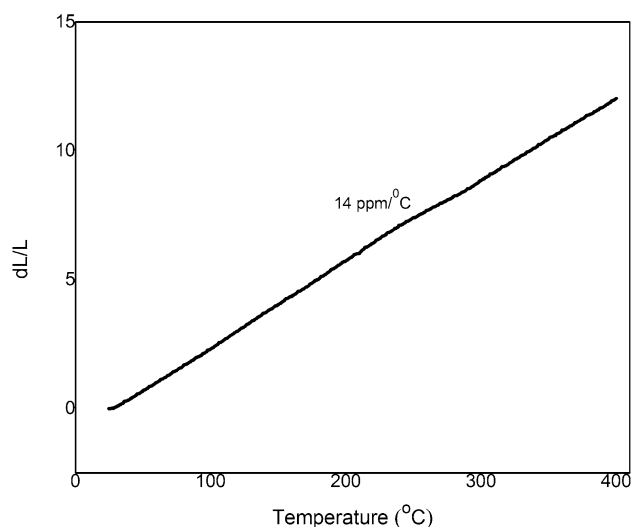


Fig. 6. Typical linear expansion curve of the BVO ceramic.

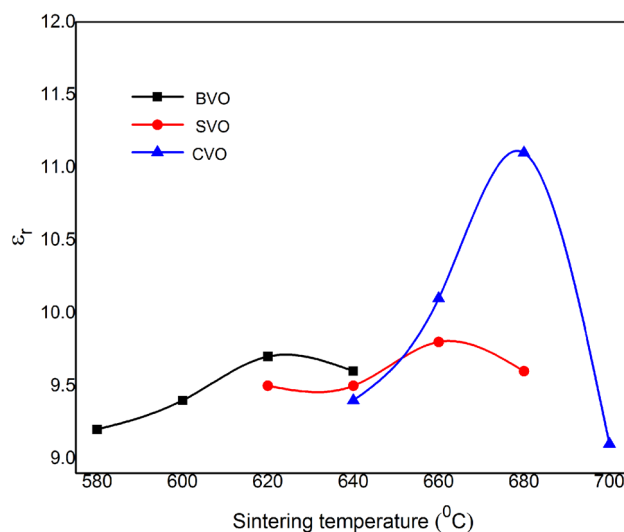


Fig. 8. Variation of dielectric constant of BVO, SVO and CVO ceramics with sintering temperature.

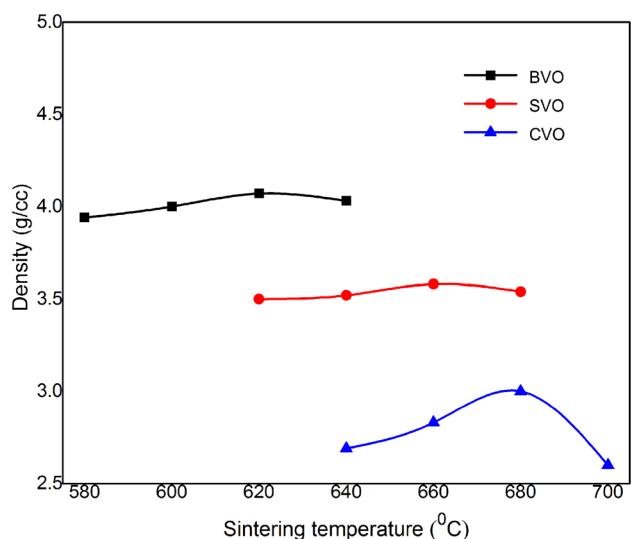


Fig. 7. Density variation of BVO, SVO and CVO ceramics with sintering temperature.

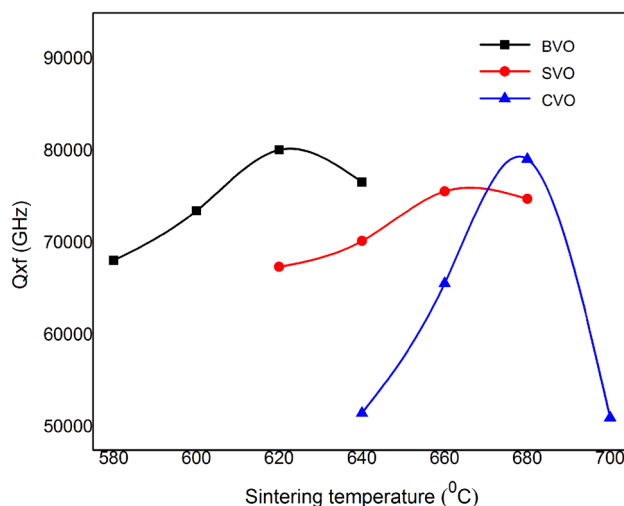


Fig. 9. Variation of quality factor of BVO, SVO and CVO ceramics with sintering temperature.

external mode vibrations observed in the BVO ceramic below  $400\text{ cm}^{-1}$  exactly matches with the  $\text{Ba}_2\text{V}_2\text{O}_7$  ceramic. One of the possibilities for the additional bands in the symmetric stretching region can be due to the presence of  $\text{V}_2\text{O}_5$  as a secondary phase since  $\text{Ba}_{16}\text{V}_{18}\text{O}_{61}$  can exist as  $8(\text{Ba}_2\text{V}_2\text{O}_7) + \text{V}_2\text{O}_5$ . We recorded the Raman spectrum of as-received  $\text{V}_2\text{O}_5$  powder separately and compared the result with that of the BVO ceramic. The Raman spectrum of  $\text{V}_2\text{O}_5$  gave rise to a strong peak at  $992\text{ cm}^{-1}$  whereas the extra modes observed in the Raman spectrum of BVO at  $916\text{ cm}^{-1}$  and  $936\text{ cm}^{-1}$ , are the typical vibrational features of the BVO ceramic as a result of different molecular arrangement. Hence, the Raman studies reveal the non-existence of the  $\text{V}_2\text{O}_5$  phase in the BVO ceramic.

In order to further confirm this result, we have separately studied the Raman spectrum of stoichiometrically mixed  $8(\text{Ba}_2\text{V}_2\text{O}_7) + \text{V}_2\text{O}_5$  powder and sintered pellets of the same at  $620^\circ\text{C}$  for 1 h to ensure the reactivity between the mixtures (Fig. 3a, b). The  $\text{Ba}_2\text{V}_2\text{O}_7$  and  $\text{V}_2\text{O}_5$  phases are seen separately in the Raman spectrum of  $8(\text{Ba}_2\text{V}_2\text{O}_7) + \text{V}_2\text{O}_5$  powder whereas the Raman spectrum of the reacted mixture of  $8(\text{Ba}_2\text{V}_2\text{O}_7) + \text{V}_2\text{O}_5$  obtained by sintering at  $620^\circ\text{C}$  for 1 h exactly matches with that of the BVO ceramic. The above result shows that the BVO ceramic existed as a single phase material at this temperature. The same behavior was also observed in the Raman spectra of the SVO<sup>21</sup> and CVO ceramics (Fig. 4a and b).

Figure 5a–c shows the SEM images of BVO, SVO and CVO ceramics sintered at optimum temperature



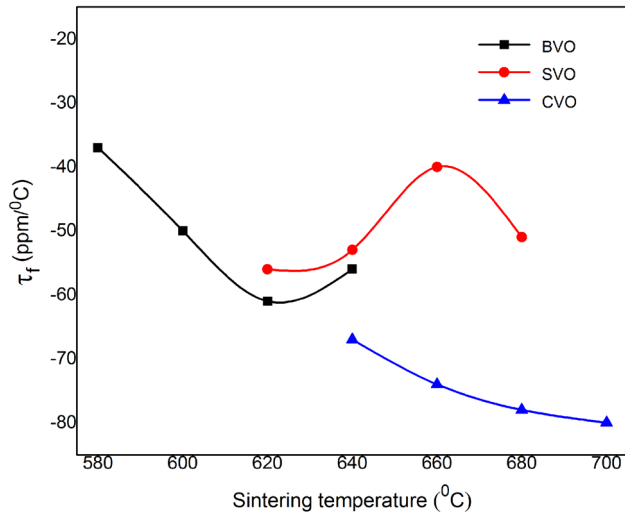


Fig. 10. Variation of temperature coefficient of resonant frequency of BVO, SVO and CVO ceramics as a function of sintering temperature.

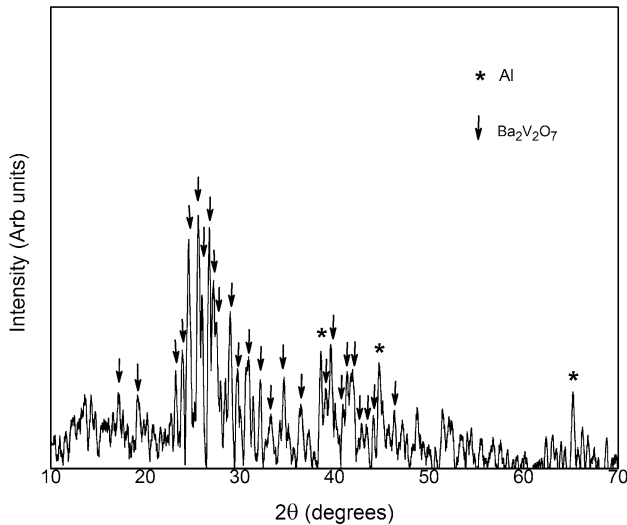


Fig. 11. XRD pattern of BVO + 20 wt.% Al ceramic sintered at 620°C for 1 h.

of 620°C, 660°C, and 680°C for 1 h, respectively. Both BVO and SVO samples show dense microstructures with well-sintered polygonal grains. A small amount of porosity was observed in the CVO ceramic as compared to the BVO and SVO ceramics. No evidence of additional phases was observed in the microstructure of these samples, which further confirms the phase purity of these ceramics. A typical linear expansion curve of the BVO ceramic is shown in Fig. 6. The BVO ceramic shows an average linear expansion coefficient of 14 ppm/°C whereas those of SVO and CVO were 14 ppm/°C and 11 ppm/°C, respectively.

Figure 7 shows the variation of density of the BVO, SVO and CVO ceramics with respect to sintering temperature. No significant variation in

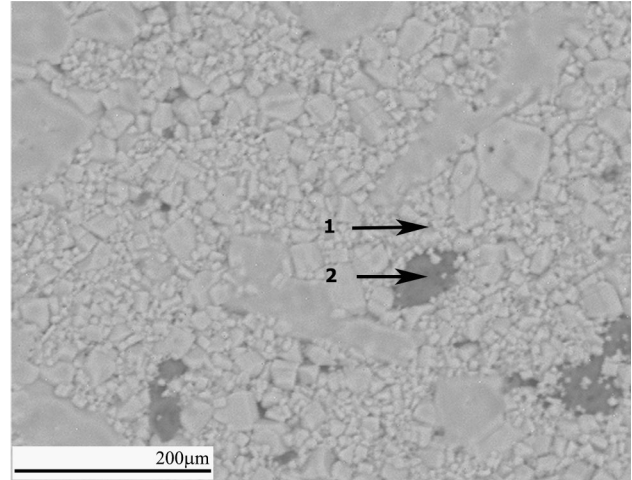


Fig. 12. Backscattered electron image of BVO + 20 wt.% Al ceramic sintered at 620°C for 1 h.

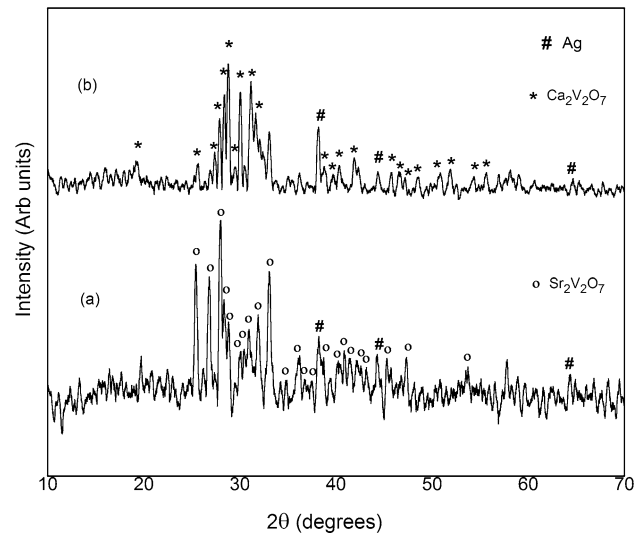


Fig. 13. X-ray diffraction patterns of (a) SVO + 20 wt.% Ag (b) CVO + 20 wt.% Ag ceramics sintered at 660°C and 680°C for 1 h.

density was observed for either BVO or SVO ceramics with increasing temperature. Maximum density values of 4.07 g/cc and 3.58 g/cc were obtained for the BVO and SVO ceramics sintered at 620°C and 660°C for 1 h, respectively, whereas the CVO ceramic exhibited a maximum density of 3.00 g/cc at 680°C for 1 h. Further increases in temperature considerably deteriorate the density of the CVO ceramic, which may be due to the evaporation of some of the constituents in the ceramic.

Figures 8 and 9 show the variation of  $\epsilon_r$  and  $Q \times f$  values of BVO, SVO and CVO ceramics sintered at different temperatures for 1 h.  $\epsilon_r$  and  $Q \times f$  values show an increasing trend with density for all the samples under study. Maximum  $\epsilon_r$  values of 9.7 and  $Q \times f$  of 80,100 GHz were observed for the BVO

**Table I. Sintering temperature, density and microwave dielectric properties of the  $A_{16}V_{18}O_{61}$  (A = Ba, Sr, Ca) and  $A_2V_2O_7$  (A = Ba, Sr, Ca) ceramics**

Compound	Sintering temperature	Density (g/cc)	$\epsilon_r$	$Q \times f$ (GHz)	Frequency (GHz)	$\tau_f$ (ppm/°C)	Reference
BVO	620°C/1 h	4.07	9.7	80,100	12.145671	-61	This work
SVO	660°C/1 h	3.58	9.8	75,600	12.124581	-40	This work
CVO	680°C/1 h	3.00	11.1	79,100	11.983492	-78	This work
Ba <sub>2</sub> V <sub>2</sub> O <sub>7</sub>	900°C/10 h	4.34	10.1	51,630	N/A	-26.5	Ref. 22
Sr <sub>2</sub> V <sub>2</sub> O <sub>7</sub>	1000°C/10 h	4.00	10.44	19,523	N/A	-34.77	Ref. 22
Ca <sub>2</sub> V <sub>2</sub> O <sub>7</sub>	950°C/10 h	3.28	12.11	15,203	N/A	-30.87	Ref. 22

N/A Not available in the respective manuscript.

sample sintered at 620°C for 1 h, whereas a  $\epsilon_r$  of 9.8 together with a  $Q \times f$  of 75,600 GHz were observed for the SVO ceramic at an optimum sintering temperature of 660°C for 1 h. The CVO ceramic shows a higher  $\epsilon_r$  compared to other ceramics. At an optimum sintering temperature of 680°C for 1 h, the CVO ceramic exhibits a  $\epsilon_r$  of 11.1 together with a  $Q \times f$  of 79,100 GHz.

Figure 10 shows the variation of  $\tau_f$  values of the BVO, SVO and CVO ceramics with sintering temperature. All the samples show negative temperature coefficients of resonant frequency. For the BVO ceramic,  $\tau_f$  values show an increasing trend with density. The sample sintered at an optimum temperature of 620°C for 1 h shows a higher  $\tau_f$  value of -61 ppm/°C. SVO and CVO ceramics have  $\tau_f$  values of -40 ppm/°C and -78 ppm/°C, respectively, at the optimum sintering temperature.

Chemical compatibility with metal electrodes is an important requirement for LTCC ceramics. In the present study, the BVO ceramic can be well sintered at 620°C for 1 h, which is in the ultra-low sintering temperature range. Therefore, an Al electrode can be used as a conducting electrode material for this ceramic. In order to study the chemical compatibility of the BVO ceramic with Al, 20 wt.% of Al powder was added to the ceramic and sintered at 620°C for 1 h. The XRD pattern of the sample sintered at this temperature is shown in Fig. 11. Aluminium peaks are separately marked and no secondary phase was observed in the XRD pattern. The SEM image (Fig. 12) shows the grains of the ceramic and Al separately without interdiffusion. EDS analysis was done on both spot 1 and spot 2 of the SEM image. In spot 1, only the presence of the BVO ceramic is noticed without interdiffusion of Al, whereas in spot 2 only Al is detected. The XRD and EDS analyses reveal that the BVO ceramic has chemical compatibility with Al electrode. In the case of the SVO and CVO ceramics, Ag can be used as an ideal electrode material since its sintering temperature is higher than the melting point of Al (660°C). To study the chemical compatibility of these ceramics with silver, 20 wt.% of Ag powder was mixed with these ceramics and sintered at 660°C and 680°C for 1 h,

respectively. The XRD patterns of the samples are shown in Fig. 13, in which, for both ceramics, the Ag peaks are marked by # and no additional phases can be seen. This result indicates the chemical compatibility of these samples with Ag electrodes.

The density and microwave dielectric properties of  $A_{16}V_{18}O_{61}$  (A = Ba, Sr, Ca) and  $A_2V_2O_7$  (A = Ba, Sr, Ca) ceramics<sup>22</sup> sintered at optimum temperatures are given in Table I.  $A_{16}V_{18}O_{61}$  ceramics can be very well sintered in the temperature range 620–680°C, which is almost 300°C less than that of  $A_2V_2O_7$ . Considerable change in the microwave dielectric properties was also observed in  $A_{16}V_{18}O_{61}$  ceramics compared to  $A_2V_2O_7$  especially in the quality factor and  $\tau_f$  values. Hence, based on the present study, it can be concluded that the existence of  $A_{16}V_{18}O_{61}$  (A = Ba, Sr, Ca) ceramic phases, which are ideally suitable for LTCC and ULTCC applications. However, further structural studies are needed to reveal the exact crystal structure of these compositions, which will be published elsewhere.

## CONCLUSION

$A_{16}V_{18}O_{61}$  (A = Ba, Sr, Ca) ceramics were prepared through the solid state ceramic route. Powder x-ray diffraction patterns of these samples showed close resemblance with that of  $A_2V_2O_7$  (A = Ba, Sr, Ca) ceramics. Laser Raman studies confirmed the phase purity of the ceramics under study. SEM analysis revealed closely packed polygonal grains with a smaller amount of porosity. An average linear expansion coefficient of 14 ppm/°C was obtained for the BVO ceramic, whereas SVO and CVO ceramics exhibited  $\alpha_L$  values of 14 ppm/°C and 11 ppm/°C, respectively. The BVO ceramic can be well sintered at an ultra-low temperature of 620°C for 1 h. The sample sintered at this temperature showed a maximum density of 4.07 g/cc together with  $\epsilon_r = 9.7$ ,  $Q \times f = 80,100$  GHz and  $\tau_f = -61$  ppm/°C. The SVO ceramic exhibited a  $\epsilon_r$  value of 9.8,  $Q \times f = 75,600$  GHz,  $\tau_f = -40$  ppm/°C at 660°C for 1 h and the CVO ceramic a  $\epsilon_r$  value of 11.1,  $Q \times f$  of 79,100 GHz and  $\tau_f$  of -78 ppm/°C at the optimum

sintering temperature of 680°C for 1 h. XRD and EDS analyses showed that the BVO ceramic has excellent chemical compatibility with an Al electrode, whereas the SVO and CVO ceramics were chemically compatible with Ag. In the present study, it has been confirmed that  $A_{16}V_{18}O_{61}$  (A = Ba, Sr, Ca) ceramics existed as single phase material and can be used as ideal candidate materials for LTCC and ULTC applications.

### ACKNOWLEDGEMENT

The authors are grateful to Dr. V. Kumar, Director, C-MET, Thrissur, for extending the facilities to carry out this work. The authors are also grateful to the Board of Research in Nuclear Sciences Mumbai for financial support under Grant No. 2013/34/13/BRNS/964.

### REFERENCES

1. C.L. Huang, M.H. Weng, and H.L. Chen, *J Mater. Chem. Phys.* 71, 17 (2001).
2. N. Santha and M.T. Sebastian, *J Mater. Res. Bull.* 43, 2278 (2008).
3. H. Zhou, X. Liu, H. Wang, and X. Chen, *J. Ceram. Inter.* 38, 367 (2012).
4. S.E. Kalathil, U.A. Neelakantan, and R. Ratheesh, *J. Am. Ceram. Soc.* 1 (2014).
5. D. Zhou, C.A. Randall, H. Wang, L.X. Pang, and X. Yao, *J. Am. Ceram. Soc.* 93, 1096 (2010).
6. G. Subodh, R. Ratheesh, M.V. Jacob, and M.T. Sebastian, *J. Mater. Res.* 23, 1551 (2008).
7. A. Feteira and D.C. Sinclair, *J. Am. Ceram. Soc.* 91, 1338 (2008).
8. N.K. James and R. Ratheesh, *J. Am. Ceram. Soc.* 93, 931 (2010).
9. E.K. Suresh, A.N. Unnimaya, A. Surjith, and R. Ratheesh, *J. Ceram. Inter.* 39, 3635 (2013).
10. M. Udovic, M. Valant, and D. Suvorov, *J. Am. Ceram. Soc.* 87, 591 (2004).
11. B. Shen, X. Yao, L. Kang, and D. Pang, *J Ceram. Int.* 30, 1203 (2004).
12. A. Surjith and R. Ratheesh, *J. Alloy Compds.* 550, 169 (2013).
13. A. Surjith, E.K. Suresh, S. Freddy, and R. Ratheesh, *J. Mat. Sci. Mat. Elec.* 24, 1818 (2013).
14. L. Fang, F. Xiang, C. Su, and H. Zhang, *J. Ceram. Inter.* 39, 9779 (2013).
15. G. Yao, P. Liu, X. Zhao, J. Zhou, and H. Zhang, *J. Eur. Ceram. Soc.* 34, 2983 (2014).
16. A.N. Unnimaya, E.K. Suresh, and R. Ratheesh, *Eur. J. Inorg. Chem.* 305 (2015).
17. B.W. Hakki and P.D. Coleman, *IRE. Trans. Microwave Theory Techn.* 8, 402 (1960).
18. J. Krupka, K. Derzakowski, B. Riddle, and J.B. Jarvis, *J Meas. Sci. Technol.* 9, 1751 (1998).
19. I.L. Botto, E.J. Baran, J. Pedregosa, and P.J. Aymonino, *J. Monat. Fur. Chem.* 110, 895 (1979).
20. A.N. Unnimaya, E.K. Suresh, J. Dhanya, and R. Ratheesh, *J. Mat. Sci. Mat. Elec.* 25, 1127 (2014).
21. E.J. Baran, I.L. Botto, J.C. Pedregosa, and P.J. Aymonino, *J. Monat. Fur. Chem.* 109, 41 (1978).
22. M.R. Joung, J.S. Kim, M.E. Song, and S. Nahm, *J. Am. Ceram. Soc.* 92, 3092 (2009).